Model Predictive Displacement Control Tuning for Tap-Water-Driven Muscle By Inverse Optimization with Adaptive Model Matching and Analysis of Contribution

Satoshi Tsuruhara (md21074@shibaura-it.ac.jp)
Shibaura Institute of Technology - Omiya Campus: Shibaura Kogyo Daigaku - Omiya Campus
https://orcid.org/0000-0002-5260-0214

Ryo Inada
Shibaura Institute of Technology - Omiya Campus: Shibaura Kogyo Daigaku - Omiya Campus

Kazuhisa Ito
Shibaura Institute of Technology - Omiya Campus: Shibaura Kogyo Daigaku - Omiya Campus

Original Article

Keywords: Adaptive model matching, Inverse optimization, Model predictive control, McKibben-type artificial muscle, Aqua drive system

Posted Date: June 28th, 2021

DOI: https://doi.org/10.21203/rs.3.rs-642585/v1

RESEARCH

Model Predictive Displacement Control Tuning for Tap-Water-Driven Muscle by Inverse Optimization with Adaptive Model Matching and Analysis of Contribution

Satoshi Tsuruhara[1*], Ryo Inada[2] and Kazuhisa Ito[3]

Abstract

The tap-water-driven McKibben muscle has many advantages and is expected to be applied in mechanical systems that require a high degree of cleanliness. However, the muscle has strong asymmetric hysteresis characteristics that depend on the load, and these problems prevent its widespread use. In this study, a novel control method - model predictive control with servomechanism based on inverse optimization with adaptive model matching - is applied to the muscle based on a high-precision mathematical model employing an asymmetric Bouc-Wen model. The experimental results show that the proposed approach achieves a high tracking performance at a reference frequency of 0.3 Hz, with a mean absolute error of 0.13 mm in the steady-state response. Furthermore, an easier controller tuning can be achieved. Additionally, the authors evaluate the contributions of the elements of the proposed method. The results show that the contribution of the adaptive system is higher than that of the servo system. Furthermore, the effectiveness of adaptive model matching is reconfirmed.

Keywords: Adaptive model matching; Inverse optimization; Model predictive control; McKibben-type artificial muscle; Aqua drive system

Nomenclature

$C_{FB}(z^{-1},k)$: feedback compensator
$C_{FF}(z^{-1},k)$: feedforward compensator
$e(k)$: muscle displacement error
$G_p(z^{-1},k)$: transfer function of linearized muscle model
$J(k)$: evaluation function
$l(k)$: muscle displacement
$\mathcal{Q}$: Block diagonal matrix consisting of $Q(i)$
$Q(i)$: weight matrices on state error $(i=1,\cdots,H_p)$
$\mathcal{R}$: Block diagonal matrix consisting of $R(i)$
$R(i)$: weight matrices on input error $(i=0,\cdots,H_u-1)$
$r(k)$: reference muscle displacement
$u(k)$: hysteresis cancelling input
$u_c(k)$: control input
$V(k)$: estimated input error vector
$V^*(k)$: optimized input vector
$V_{fv}(k)$: favorite control input
$v(k)$: control input error
$\boldsymbol{x}(k)$: state vector of augmented system
$\boldsymbol{x}_p(k)$: state vector of linearized muscle system
$\boldsymbol{x}_r(k)$: state vector of reference system
$\boldsymbol{x}_s(k)$: state vector of servo compensator system
$y_{hy}(k)$: virtual hysteresis variable
$\boldsymbol{\theta}_0$: parameter vector of the muscle system
$\Xi(k)$: estimated state error vector
$\boldsymbol{\xi}(k)$: state vector of error system
$\boldsymbol{\phi}(k)$: regressor vector

ABW : asymmetric Bouc-Wen
AMPCS : adaptive model predictive control with servomechanism
LTI : linear time invariant
MPC : model predictive control
MPCS : model predictive control

*Correspondence: md21074@shibaura-it.ac.jp
[1]Graduate School of Mechanical Engineering, Shibaura Institute of Technology, 307 Fukasaku, Minuma, Saitama 3378570, Japan
Full list of author information is available at the end of the article

	with servomechanism
MPCS with AL	: MPCS with adaptive linearization
MPCS with AMM	: MPCS with adaptive model matching
MPC with AMM	: MPC with adaptive model matching
NRMSE	: normalized root mean square error
RLS	: recursive least square
SBW	: standard Bouc-Wen

1 Introduction

The McKibben-type artificial muscle has been widely researched in biorobotic engineering, medical engineering, and industrial applications, owing to its many advantages including high flexibility, high power density, low weight, low cost, and simple structure [1]. Furthermore, aqua drive systems present several other advantages such as absence of fire hazards, a small burden on the environment and convenient disposability. In addition, tap-water-driven systems are readily available because they do not require compressors and special facilities such as power sources and can be directly actuated through a typical water supply network [2][3]. Therefore, tap-water-driven muscles have the advantages of both the McKibben muscles and tap-water-driven system, and are expected to be used in the above-mentioned applications that require a high degree of cleanliness. However, the muscle is well-known to have strong asymmetric hysteresis characteristics caused by the nonlinear contraction behavior and friction between components. In addition, its characteristics depend on the load applied to the muscle. Moreover, the muscle is driven by tap water pressure that may vary to some extent depending on the time of the day, and there is a significant change in the characteristics of the system depending on the individual muscle. Therefore, it is a major challenge to derive a precise muscle model that describes its behavior and to design a controller for high-performance displacement control.

To design such a controller, most of the previous studies have already proposed model-based control such as model reference adaptive control [4], sliding mode control [5], and H_∞ control [6]. However, it is difficult to achieve high control performance because these control methods adopt linear models despite the strong nonlinearity of the muscle and do not consider practical input saturation in the design step. Furthermore, nonlinear model-based control has also been applied to muscle systems [7][8]. However, the control strategies are more complex, and the parameter identification is also moderately challenging because of the adaptation of the model based on the first-principles model.

Three representative models - the Prandtl-Ishlinskii model, Preisach model, and Bouc-Wen model - have been proposed to describe the nonlinearities of the muscle [9][10][11]. Among the three models, the Bouc-Wen model has a simple structure and consists of linear and nonlinear parts that makes it suitable for control.

In this study, the modeling and the controller design are discussed for a tap-water-driven McKibben-type artificial muscle, followed by a detailed analysis of the proposed system. An asymmetric Bouc-Wen model describing the asymmetricity of the hysteresis property was introduced, and a relatively simple and accurate model was obtained [12]. Subsequently, a linear model of the muscle was obtained based on a hysteresis cancelation input using the inverse model of the asymmetric Bouc-Wen model and an adaptive algorithm. An adaptive model predictive controller with servomechanism (AMPCS) [13][14] that was introduced to identify the change in the characteristics of the muscle load online, was applied. This controller not only considers the constraint of the valve input voltage, but also uses an adaptive system to compensate for the modeling errors and achieves a high control performance. However, the control performance obtained by the proposed approach depends strongly on the weight matrices in the evaluation function. Furthermore, the tuning of the weight matrices in the evaluation function was determined by considerable trial and error, because the relationship between the obtained control performance and weight matrices was not trivial. To overcome these problems, an inverse optimization technique is applied to obtain the appropriate weight matrices directly. Subsequently, the model predictive controller using the obtained weights behaves similar to the prespecified favorite controller. However, this method assumes an LTI system, owing to two critical problems: solvability and calculation in real-time execution. Therefore, it is not possible to combine the AMPCS controller, wherein the predictor is updated at each step, and the inverse optimization technique. To solve this problem, an adaptive model matching (AMM) technique is proposed by matching a linearized muscle model with a pre-specified LTI predictor, and the effectiveness of the proposed technique is confirmed through numerical simulation and experimentation [15][16]. Moreover, it is unclear that the element of the control system contributes most to the control performance because the control system has become so complex. Therefore, two control methods are considered in addition to the previous studies to clarify them.

The contributions of this paper are the following: 1) A highly accurate mathematical model based on

the asymmetric Bouc-Wen model is derived, and high NRMSE is achieved. 2) The linearization method is proposed based on the highly accurate mathematical model. 3) An inverse optimization method is proposed to reduce the controller-tuning routines. 4) Using an adaptive model matching, the adaptive system and the inverse optimization algorithm can be used together, and a control system that is robust to load variations is achieved. 5) The contribution of the elements of the complex system was evaluated and clarified.

The remainder of this paper is organized as follows. First, the modeling of the tap-water-driven muscle is described based on the asymmetric Bouc-Wen model. The model predictive controller, designed to achieve easier controller tuning through inverse optimization, is subsequently described. Next, the AMM is introduced to enable the use of both the adaptive system and inverse optimization. Moreover, the experimental results and statistical evaluations, showing the effectiveness and robustness of the proposed controller, are presented. Finally, the contribution of the elements of the control system are evaluated by implementing four control strategies. Accordingly, the elements and control strategies that perform excellently are quantitatively examined.

2 Modeling of Tap-Water-Driven Muscle and Estimation of Its Parameter

In this section, the system to be considered is modeled, and the parameter estimation results are presented.

2.1 Modeling of tap-water-driven muscle using asymmetric Bouc-Wen model

Several asymmetric Bouc-Wen models have already been proposed for describing the hysteresis characteristics of plants. In this study, a previously proposed asymmetric Bouc-Wen model [3] is adopted owing to its simple structure. However, the asymmetric Bouc-Wen model is described based on differential equations, and the MPC approach in the discrete time domain cannot be directly applied. Therefore, the asymmetric Bouc-Wen model is rewritten in the discrete time domain with a forward difference approximation [17]. In this study, the muscle dynamics based on the asymmetric Bouc-Wen model are obtained as follows:

$$\begin{cases} l(k) = a_1 l(k-1) + a_2 l(k-2) + b_1 u(k-1) + y_{ahy}(k) \\ y_{ahy}(k) = \sum_{i=1}^{m} c_i y_{ahy}(k-i) \\ y_{ahy}(k-i) = A_i\{l(k-i) - l(k-1-i)\} \\ \quad - \beta_i |l(k-i) - l(k-1-i)||y_{ahy}(k-1-i)|^{n-1} \\ \quad - \gamma_i\{l(k-i) - l(k-1-i)\}|y_{ahy}(k-1-i)|^{n} \\ \quad + y_{ahy}(k-1-i) + g(l(k-i)) \\ g(l(k-i)) = \sum_{j=2}^{p} h_{ji} l^j(k-i) \end{cases} \tag{1}$$

where the variable $l(k)$ is the displacement of the muscle, $y_{hy}(k)$ is the virtual hysteresis variable, a_1, a_2, b_1 are linear parameters and $A_i, \beta_i, \gamma_i, c_i$ are hysteresis parameters and $i = 1, 2$ in Equation 1.

In addition, the nonlinear function $g(l(k))$ represents the asymmetricity of hysteresis; h_{ij} are its parameters and $i = 1, 2, n = 3$ in Equation 1. Note that the proposed model expresses not only the muscle dynamics but also the proportional valve dynamics. In this study, Equation 1 expresses the muscle model that combines a linear model with the discretized asymmetric Bouc-Wen model. Specifically, the proposed model incorporates the linear model corresponding to the first and third terms and the asymmetric Bouc-Wen model corresponding to the fourth and fifth terms in the first equation. Note that a standard Bouc-Wen model is expressed as Equation 1 without a nonlinear function $g(l(k))$ that comprises the polynomial function of muscle displacement.

2.2 Parameter estimation and linearization with recursive least square (RLS) algorithm

An RLS algorithm corresponding to online identification is adopted for the proposed muscle model in Equation 1 and for the following equation:

$$l(k) = \boldsymbol{\phi}^T(k-1)\boldsymbol{\theta}_0 \tag{2}$$

where $\boldsymbol{\phi}(k), \boldsymbol{\theta} \in \mathbb{R}^{15}$ represent the regressor and true value vector, respectively. In particular, parameter estimation has been performed in a previous study [14] assuming that $y_{hy}(k)$ is the difference between the displacement of the muscle and the output of the linear model; that is, $y_{hy}(k) = l(k) - [a_1 l(k-1) + a_2 l(k-2) + b_1 u(k-1)]$ because $y_{hy}(k)$ cannot be measured because of the virtual variable [17]. In addition, a linearization model for the proposed muscle model is obtained by

canceling the hysteresis term, with $u(k)$ defined as

$$u(k) = u_c(k) - \frac{1}{\hat{b}_1(k)} \left(y_{hy}(k) + y_{hy}(k-1) \right) \quad (3)$$

where $\hat{b}_1$ denotes the estimated parameter of b_1 and the input $u_c(k)$ is designed later. By applying a hysteresis-canceling input $u(k)$, the linearized model is obtained under the condition that the RLS algorithm provides an appropriate estimation:

$$l(k) = \hat{a}_1(k-1) + \hat{a}_2(k-2) + \hat{b}_1 u_c(k-1) \quad (4)$$

where $\hat{a}_1, \hat{a}_2, \hat{b}_1$ denote the estimated values of the corresponding parameters in Equation 1.Note that a constrained RLS algorithm is adopted to avoid the division of Equation 3 by zero.

2.3 Evaluation of the proposed model

In this section, the evaluation of the proposed muscle model is described. The parameter of the muscle model in Section 2.1 was estimated by the method described in Section 2.2.

Figure 1 shows the experimental circuit and Figure 2 shows the experimental equipment. The setup consists of the McKibben-type artificial muscle, two proportional valves, a linear encoder, and a PC. The muscle is contracted by tap water pressure. Here, the proportional valve is a flow control system, and its flow rate is controlled by the input voltage $u(k)$. The linear encoder measures the displacement $l(k)$ of the muscle and sends it to the controller. These details are summarized in Table 1. Using this experimental setup, the muscles are modeled and the control experiments are performed in Section 5.

Figure 1 Experimental circuit

Figure 2 Experimental setup

Figure 3 and 4 show the comparison of the time response and hysteresis loop, respectively, among the proposed asymmetric Bouc-Wen model(Equation 1), the standard Bouc-Wen model, and the measured experimental results. Figure 3 also shows the linear model that consists of only the linear part of Equation 1. These results show that the asymmetric Bouc-Wen model fits the measurements with a higher accuracy than the other models. In addition, Table 2 shows the NRMSE comparison for several step-ahead predictions among the three models: the asymmetric Bouc-Wen model, standard Bouc-Wen model, and linear model that consists of only the linear part of Equation 1. From the table, it can be seen that the proposed model maintains a higher NRMSE even for five step-ahead and simulated output predictions, although the other models lose their precision.

Table 1 Components of the experimental circuit

Item	Specifications
Proportional valves	KFPV300-2-80, Koganei Corporation C_v Value: 1.6; range of input voltage: 0 to 10 V
Linear encoder	DX-025, MUTOH Industries Ltd. Resolution: 0.01 mm
PC	Operating system: Windows 7, Microsoft Corporation CPU (Core i5): 3.10 GHz, RAM: 4.00 GB Applications: MATLAB/Simulink and dSPACE 1103
Tap-water-driven muscle	In-house custom-built muscle Length: 360 mm
Tap-water	Average supply pressure: 0.15 MPa (G)

Figure 3 Comparison of temporal responses associated with each muscle model and the experimental results

Figure 4 Comparison of hysteresis loop of each muscle model and the measurement results

Table 2 Comparison of NRMSE of each muscle model and the measurement results

Prediction	NRMSE [%]		
	ABW model	SBW model	Linear model
1-step ahead	99.8	99.8	97.5
3-step ahead	98.8	98.6	90.2
5-step ahead	97.4	96.7	83.1
Simulated output	95.7	86.2	51.5

3 Model Predictive Controller Design with Inverse Optimization

In the previous section, the linearized muscle model in Equation 4 was obtained based on the RLS algorithm and hysteresis-canceling input. Therefore, model predictive control, including an adaptive and servo system was applied, and a high control performance was achieved, as shown in [13][14]. Here, it is important to perform weight tuning in the evaluation function of model predictive control, to achieve improved control performance. However, in practice, these weights

are usually obtained by trial and error because the relationship between each weight and closed-loop frequency domain characteristics, including sensitivity and robustness, is not intuitive in the design step. This requires a time-consuming routine and prevents model predictive control from being widely used in practical applications. To solve this problem, Cairano and Bemporad proposed an inverse optimization technique [18] in 2009 to obtain weight matrices based on the fact that the model predictive control behaves similar to designed favorite state feedback controller when constraints are not active. Note that the favorite feedback controller can be designed using a pole placement controller, as described in Section 3.3. Therefore, the turning of weight matrices in the evaluation function of the model predictive control can be easily accomplished, and a high control performance can be achieved. In addition, an appropriate state reset of the servo compensator is also introduced to avoid the wind-up phenomenon.

3.1 Derivation of the error system

Consider the following system, described as a linearized, discrete-time state-space model of plants.

$$\begin{cases} \boldsymbol{x}_p(k+1) = A_p\boldsymbol{x}(k) + \boldsymbol{b}_p u_c(k) \\ \quad\quad l(k) = \boldsymbol{c}_p\boldsymbol{x}_p(k) \end{cases} \tag{5}$$

where $x_p \in \mathbb{R}^{n_p}$ is the state vector of the linearized muscle. In addition, the reference signal is generated based on the following equation:

$$\begin{cases} \boldsymbol{x}_r(k+1) = A_r\boldsymbol{x}_r(k) \\ \quad\quad r(k) = \boldsymbol{c}_r\boldsymbol{x}_r(k) \end{cases} \tag{6}$$

where $x_r \in \mathbb{R}^{n_r}$ and $r(k) \in \mathbb{R}$ are the states of reference and reference, respectively. It is assumed that the eigenvalues of the matrix A_r exist on the unit circle in the complex plane. The designer can generate various types of reference signals, including step, periodic, and ramp signals by selecting the appropriate $A_r \in \mathbb{R}^{n_r\times n_r}$ and $c_r \in \mathbb{R}^{n_r}$. For the tracking problem, the servo compensator including the internal model, is inserted into the controller.

$$\begin{cases} \boldsymbol{x}_s(k+1) = A_s\boldsymbol{x}_s(k) + \boldsymbol{b}_s e(k) \\ \quad\quad e(k) = r(k) - l(k) \end{cases} \tag{7}$$

where $x_s \in \mathbb{R}^{n_s}$ is a state vector of the servo compensator and $n_r \leq n_s$ should be satisfied. Here, $A_s \in \mathbb{R}^{n_s\times n_s}$ includes all the modes of reference signals to satisfy the internal model principle. Therefore, it is set as $A_s = A_r$ in this study. System Equation 5-7 can be rewritten as the following augmented system:

$$\begin{cases} \boldsymbol{x}(k+1) = A\boldsymbol{x}(k) + \boldsymbol{b}u_c(k) + E\boldsymbol{x}_r(k) \\ \quad\quad e(k) = \boldsymbol{c}\boldsymbol{x}(k) + \boldsymbol{c}_r\boldsymbol{x}_r(k) \end{cases} \tag{8}$$

where $x(k) = [\boldsymbol{x_p}^T(k)\ \boldsymbol{x_s}^T(k)]^T \in \mathbb{R}^{n_p+n_s}$ is the augmented state vector and

$$A = \begin{bmatrix} A_p & \boldsymbol{0} \\ -\boldsymbol{b}_s\boldsymbol{c}_p & A_r \end{bmatrix},\ \boldsymbol{b} = \begin{bmatrix} \boldsymbol{b}_p \\ \boldsymbol{0} \end{bmatrix},\ \boldsymbol{c} = \begin{bmatrix} -\boldsymbol{c}_p & \boldsymbol{0} \end{bmatrix},$$

$$E = \begin{bmatrix} O_{n\times n_r} \\ \boldsymbol{b}_s\boldsymbol{c}_r \end{bmatrix},\ \boldsymbol{x}(k) = \begin{bmatrix} \boldsymbol{x}_p(k) \\ \boldsymbol{x}_s(k) \end{bmatrix}$$

For the augmented system (Equation 8), the linear error feedback regulator problem is solvable only if there exist matrices $\Pi \in \mathbb{R}^{(n_p+n_s)\times n_r}$ and $\Gamma^T \in \mathbb{R}^{n_r}$ that satisfy the following regulator equation [19]:

$$\begin{cases} \Pi A_r = A\Pi + \boldsymbol{b}\Gamma + E \\ \quad 0 = \boldsymbol{c}\Pi + \boldsymbol{c}_r \end{cases} \tag{9}$$

It is assumed that matrices Π and Γ exist that satisfy Equation 9. By defining the state vector of the error system, $\boldsymbol{\xi}(k) = \boldsymbol{x}(k) - \Pi\boldsymbol{x}_r(k)$ and $v(k) = u_c(k) - \Gamma\boldsymbol{x}_r(k)$, the following error system can be derived:

$$\begin{cases} \boldsymbol{\xi}(k+1) = A\boldsymbol{\xi}(k) + \boldsymbol{b}v(k) \\ \quad\quad e(k) = \boldsymbol{c}\boldsymbol{\xi}(k) \end{cases} \tag{10}$$

In the following discussion, Equation 10 is utilized.

3.2 MPCS design with error system

The evaluation function in MPCS for the error system, Equation 10, is described as

$$\begin{aligned} V(k) &= \sum_{i=1}^{H_p} \|\hat{\boldsymbol{\xi}}(k+i|k)\|^2_{Q(i)} + \sum_{i=0}^{H_u-1} \|\hat{v}(k+i|k)\|^2_{R(i)} \\ &= \|\Xi(k)\|^2_{\mathcal{Q}} + \|V(k)\|^2_{\mathcal{R}} \end{aligned} \tag{11}$$

where H_p,H_u are the prediction and control horizons, respectively, and the estimated signal vectors $\Xi(k)$,$V(k)$, are defined as follows:

$$\Xi(k) = \begin{bmatrix} \hat{\boldsymbol{\xi}}(k+1|k) \\ \vdots \\ \hat{\boldsymbol{\xi}}(k+H_p|k) \end{bmatrix},\ V(k) = \begin{bmatrix} \hat{v}(k|k) \\ \vdots \\ \hat{v}(k+H_u-1|k) \end{bmatrix}$$

where $\mathcal{Q} \geq 0, \mathcal{R} > 0$ are the weight matrices consisting of weight matrices $Q(i)$ $(i = 1, \cdots, H_p)$ and $R(i)$ $(i = 0, \cdots, H_u - 1)$. Let $H_p = H_u$ for simplicity. Accordingly, the result of the model prediction control under unconstrained conditions provides an optimized input vector as follows:

$$V^*(k) = -(S^T \mathcal{Q} S + \mathcal{R})^{-1} S^T \mathcal{Q} T \boldsymbol{\xi}(k) \tag{12}$$

where

$$\mathcal{T} = \begin{bmatrix} A \\ A^2 \\ \vdots \\ A^{H_p} \end{bmatrix}, \ \mathcal{S} = \begin{bmatrix} \boldsymbol{b} & \mathbf{0} & \cdots & \mathbf{0} \\ A\boldsymbol{b} & \boldsymbol{b} & \cdots & \mathbf{0} \\ \vdots & \vdots & \ddots & \vdots \\ A^{H_p-1}\boldsymbol{b} & A^{H_p-2}\boldsymbol{b} & \cdots & \boldsymbol{b} \end{bmatrix}$$

3.3 Inverse optimization method for MPCS

In the inverse optimization technique, the optimal weight matrices in the evaluation function of MPCS are obtained by solving Problem 1.

Problem 1 (MPCS matching): Assume that a pair (A, b) is reachable. For a pre-assigned '' favorite controller '' with state feedback,

$$V_{fv} = \bar{K}\boldsymbol{\xi}(k), \ \bar{K} \in \mathbb{R}^{H_u \times n} \tag{13}$$

determines that the weights that have the unconstrained MPCS solution, Equation 12, for the evaluation function, Equation 11, are equal to those of the favorite controller, Equation 13, that is, $V_{fv}(k) = -(S^T \mathcal{Q} S + \mathcal{R})^{-1} S^T \mathcal{Q} T \boldsymbol{\xi}(k)$. □

Assuming that the same state feedback K was used along the entire prediction horizon, the estimations of the predicted state can be expressed as follows:

$$\begin{aligned} \boldsymbol{\xi}(k + H_u) = A(A + \boldsymbol{b}K)^{H_u-1}\boldsymbol{\xi}(k) \\ + \boldsymbol{b}K(A + \boldsymbol{b}K)^{H_u-1}\boldsymbol{\xi}(k) \end{aligned} \tag{14}$$

Therefore, Problem 1 is immediately solved if weights $\mathcal{Q}$ and $\mathcal{R}$ can be determined in Equation 11 satisfying

$$-(\mathcal{R}+\mathcal{S}^T\mathcal{Q}\mathcal{S})^{-1}\mathcal{S}^T\mathcal{Q}\mathcal{T} = \begin{bmatrix} K \\ K(A\boldsymbol{b}K) \\ \vdots \\ K(A + \boldsymbol{b}K)^{H_u-1} \end{bmatrix} = \bar{K} \tag{15}$$

Equation 15 is not trivial because each weight has a constraint, such as $\mathcal{Q} \geq 0, \mathcal{R} > 0$. Therefore, the following convex problem should be solved based on the LMI approach, to obtain the solution to Problem 1:

$$\begin{aligned} J^* = \min_{\mathcal{Q},\,\mathcal{R}} & \|(\mathcal{R} + \mathcal{S}^T\mathcal{Q}\mathcal{S})\bar{K} + \mathcal{S}^T\mathcal{Q}\mathcal{T}\| \\ \text{s.t.} \quad & R(i) > 0, \ i = 1, \ldots, H_u \\ & Q(i) \geq 0, \ i = 1, \ldots, H_p \end{aligned} \tag{16}$$

The optimal $\mathcal{Q}$,$\mathcal{R}$ values are obtained by solving Equation 16. If the optimum of Equation 16 achieves $J^* \simeq 0$, the MPCS controller using the obtained weights behaves similar to the favorite controller, Equation 13, when the constraints are not active. Note that this inverse optimization is performed offline, and its process is considered to correspond to the unconstrained MPCS controller design. However, the MPCS controller, intended to generate the optimal control input based on the obtained $\mathcal{Q}$,$\mathcal{R}$, is online, and its process is considered to correspond to the constrained design.

3.4 State reset of servo compensator

In addition, to the inverse optimization, the state reset of the servo compensator is also considered for the integrator wind-up. Therefore, in this study, the state reset of the servo compensator is introduced at each step until the evaluation function has a value smaller than the prespecified threshold [20]. The state reset has the potential to preserve high control performance. However, this threshold is selected independent of the weights, by trial and error. A smaller threshold blocks the servomechanism owing to the frequent servo state reset. In contrast, for a larger value, wind-up occurs easily.

4 Adaptive model matching

In Section 3, an MPCS controller with inverse optimization is proposed. However, the system is assumed to be an LTI system because this method requires solvability and calculation to solve inverse optimization in real-time execution provided that the adaptive algorithm is applied. First, the obtained model, Equation 4, is a time-varying system because the adaptive system is active. Therefore, the solvability of the regulator equation, Equation 9, may not be guaranteed. Second, the weights obtained by the inverse optimization of $\mathcal{Q}$,$\mathcal{R}$ should be recalculated at every step owing to the updating of the parameters and it is impossible to achieve both in practice. To overcome these problems, the AMM is introduced to compensate for the error between the linearized muscle system and the fixed predictor in MPCS. Dynamical feedback and feedforward compensators are introduced to place poles and zeros to match the pre-specified predictor in the MCPS controller. A conceptual schematic of the AMM is shown in Figure 5.

Figure 5 Conceptual schematic of adaptive model matching (AMM) compensator

In the figure, $C_{FF}(k)$,$C_{FB}(z^(-1),k)$ represent the dynamical feedforward and feedback compensators, respectively. $G_p(z^(-1),k)$ is obtained based on the linearized muscle model according to Equation 4 and is defined as

$$G_p(z^{-1},k) = \frac{\hat{b}_1(k)z^{-1}}{1+\hat{a}_1(k)z^{-1}+\hat{a}_2(k)z^{-2}} \tag{17}$$

where z^{-1} is the unit time delay operator and $\hat{}$ is the estimated value of Equation 1. Moreover, the prespecified LTI predictor, $G_d(z^{-1})$ has the same structure as Equation 17, that is,

$$G_d(z^{-1}) = \frac{b_{d1}z^{-1}}{1+a_{d1}z^{-1}+a_{d2}z^{-2}} \tag{18}$$

in the MPCS controller. Therefore, from Figure 3, the following equation should be held:

$$\frac{\{1+C_{FF}(z^{-1},k)\}G_p(z^{-1},k)}{1+G_p(z^{-1},k)C_{FB}(z^{-1},k)} \tag{19}$$

To satisfy the relationship in Equation 19, the adaptive compensator is defined as

$$\begin{cases} C_{FF}(z^{-1},k) = \dfrac{b_{d1}}{\hat{b}_1(k)} \\ C_{FB}(z^{-1},k) = \dfrac{a_{d1}+\hat{a}_1(k)}{b_{d1}} + \left(\dfrac{a_{d2}+\hat{a}_2(k)}{b_{d1}}\right) z^{-1} \end{cases} \tag{20}$$

Therefore, using Equation 20, the pre-specified LTI predictor and the linearized muscle system are matched adaptively. In addition, the entire block diagram combining the MPCS designed in Section 3 and the AMM proposed in this study is shown in Figure 6. Note that not only AMM (Equation 20), but also adaptive linearization (Equation 3) is contained in the green range. Therefore, the constraint on the valve input voltage is modified as follows:

$$\begin{aligned} 0 \le\ & C_{FF}(k)[u_c(k+i|i) - C_{FB}(z^{-1},k)l(k)] \\ & - \frac{1}{\hat{b}_1(k)}\hat{y}_{hy}(k+1) \le 10 \end{aligned} \tag{21}$$

where $i = 0, 1, \cdots, H_u - 1$

Figure 6 Block diagram of MPCS with AMM

5 Experimental results and discussions

In this section, the experimental conditions are described, and a comparison between MPCS with and without AMM, based on the experimental results, is presented. However, the MPCS with AMM is composed of a servo compensator, adaptive model matching, and adaptive linearization. Therefore, to evaluate the contribution of each element to the control performance, the performance of four control strategies is compared: MPCS, MPCS with AMM, MPC with AMM that has zero influence of the servo system, and MPCS with AL that introduces only adaptive linearization without AMM.

5.1 Experimental conditions

In this experiment, first, MPCS and MPCS with AMM are compared. Next, MPC with AMM and MPCS with AL are compared along with MPCS and MPCS with AMM, to evaluate the contribution of the servo system, AMM, and adaptive linearization. Here, MPC with AMM is realized by always performing a state reset to eliminate the effect of the servo system, whereas MPC with AL is only performed with adaptive linearization. It should be noted that the objective of this experiment is to obtain a high control performance even in the presence of modeling errors due to loading. Therefore, the load applied to the muscle is 68 N; however, the initial parameters of the muscle model are obtained through experiments under a load of 44N for all control strategies, and they are used as the initial parameters of the hysteresis-canceling input (Equation 3), AMM compensator (Equation 20), and predictor (Equation 18). These are set as shown in Table 3.

Table 3 Parameter for experiment under a load of 44 N

Parameter	Value
a_1	1.124
a_2	−0.296
b_1	0.685
A_1	−3.309
A_2	−5.207
β_1	0.141
β_2	−0.301
γ_1	0.574
γ_2	−0.681
c_1	0.110
c_2	0.105
h_{21}	0.075
h_{22}	−0.039
h_{31}	-6.745×10^{-4}
h_{32}	-3.117×10^{-4}
$offset$	−0.800

For this system, a sinusoidal reference signal was applied at an amplitude of 20 mm, offset of 30 mm,

and frequency of 0.1–0.3 Hz, with a sampling time of 0.1 s. The predictive horizon and control horizon were both set to 5, and the state reset threshold for the evaluation function was set to 500 for MPCS with AMM, zero for MPC with AMM, and the other threshold was not applied. The reason for not applying the state reset is that modeling error always occurs owing to the lack or insufficiency of adaptive compensation, and the frequent resets may lead to performance degradation. The state feedback gain K is designed such that the pole placement $A + \boldsymbol{b}K$ in Equation 13 has the desired eigenvalues:$\{0.5, 0.6, 0.8 \pm 0.5i, 0.8\}$in MPCS and$\{0.6, 0.8, 0.8 \pm 0.5i, 0.9\}$in the other control strategies. This assignment of the poles enhance the effectiveness of the adaptive algorithm and servo compensator on the control performance. The adaptive algorithm is more dominant in preliminary experiments, and the servo compensator may interfere with the operation of the adaptive algorithm. Therefore, the poles of these control strategies were placed closer to 1, compared with the poles of MPCS. The results of inverse optimization numerically calculated using the software YALMIP [21] provide $J^* = 8.462 \times 10^{-12}$ in MPCS and $J^* = 2.563 \times 10^{-10}$ in the other control strategies, respectively. Therefore, the designed controller can be considered to behave as an MPCS controller, using the optimized weights $\mathcal{Q}$ and $\mathcal{R}$ as the favorite controller. A code for real-time control was generated using the code generator CVXGEN [22].

5.2 Comparison between MPCS with and without AMM

Figure 7 and 8 compare the tracking control performance between MPCS and MPCS with AMM over a reference signal of 0.3 Hz. These figures show the tracking control performance improvement of the MPCS with AMM over a MPCS without AMM. Although the transient response of the MPCS with AMM is degraded for adaptation in Figure 7, Figure 8 shows a considerably smaller tracking error in the steady-state response. This is owing to the smaller prediction error shown in Figure 9 that can be explained by the fact that the designed AMM compensator performs suitably. In contrast, in the MPCS with a fixed predictor, the servomechanism reduce the tracking error, nonetheless the prediction error remains. Figure 10 shows the control input for the MPCS and MPCS with AMM. Although the generated control input is oscillatory because of the adaptive system in the transient response, it is observed to satisfy the constraint on the valve input voltage in the entire range.

Figure 11 shows box plots at each reference frequency in the mean absolute error. From this figure, it can be seen that, on one hand, the control performance of the MPCS degrades as the target frequency increases. On the other hand, the control performance of MPCS with AMM is maintained even when the frequency is increased. Moreover, the maximum value of MPCS with AMM is less than the minimum value of MPCS. Therefore, MPCS with AMM can be confirmed to be robust to frequency changes than the MPCS without AMM.

Figure 7 Comparison of tracking performances between MPCS with and without AMM

Figure 8 Comparison of tracking performances between MPCS and MPCS with AMM for the steady-state response

Figure 9 Comparison of prediction errors between MPCS with and without AMM for the steady-state response

Figure 10 Comparison of control inputs between MPCS with and without AMM

Figure 11 Comparison of box plots for MPCS and MPCS with AMM

5.3 Contribution analysis of servo ans adaptive system

In this section, to analyze the contribution of the servo and adaptive systems, the three control strategies - MPCS, MPCS with AMM, and MPC with AMM - are compared. Figure 12 shows a box plot comparing the three control strategies. From this figure, it can be observed that, the MPC with AMM has a higher control performance than MPCS at all the frequencies considered. This result implies that the contribution of the adaptive system is higher than that of the servo system at all the frequencies considered. In particular, at high frequencies, the contribution of the adaptive system is large.

In addition, comparing MPC with AMM and MPCS with AMM, it can be seen that there is no difference in the performance of MPC with AMM and MPCS with AMM at low frequencies; however, there is a performance difference at high frequencies. This is because the servo system interferes with the performance of the adaptive system. Figure 13 shows the comparison of the prediction error at 0.3 Hz. The result shows that the prediction error of MPC with AMM is smaller than that of MPCS with AMM.

Figure 12 Comparison of box plots for investigating the contribution of servo and adaptive systems

Figure 13 Comparison of prediction errors between MPCS with AMM and MPC with AMM

Figure 14 Comparison of MPCS with AL in each evaluation interval

Figure 15 Comparison of box plots for evaluating the contribution of adaptive linearization and adaptive model matching

5.4 Contribution analysis of adaptive model matching and adaptive linearization

In this section, to analyze the contribution of adaptive model matching and adaptive linearization, the three control strategies - MPCS, MPCS with AMM, and MPCS with AL - are compared. To this end, it is necessary to determine an appropriate evaluation interval that will result in a steady-state response of the MPCS with AL. This is because in this study, when updating the adaptive algorithm, the hysteresis term is obtained by subtracting the linear term from the measured data, as explained in modeling in Section 3, and the time to reach steady-state response may be longer in MPCS with AL than in the other control schemes due to the fact that adaptive model matching has not been introduced. For a target trajectory of 0.1 Hz, the results were evaluated at five evaluation intervals of 20-40, 40-60, 60-80, 80-100, and 100-120 s, and the box plots are shown in Figure 14. The results show that when the evaluation interval is 20-40 that is the same as the other control strategies, the control performance is not steady yet for the outliers; however, when the evaluation interval is shifted backward, the control performance is improved and steady. Therefore, the MPCS with AL is compared with the other control methods based on an evaluation interval of 100-120 s.

Figure 15 shows a box plot comparing the three control strategies: MPCS, MPCS with AMM, and MPCS with AL. From these results, it can be confirmed that the performance of MPCS with AL is higher than that of the MPCS at high frequencies, although the performances of MPCS and MPCS with AL are almost equal when the target trajectory is at low frequencies. This can be attributed to the fact that the contribution of the servo system is smaller and that of the adaptive system is higher at high frequencies, as revealed in the previous section. Furthermore, comparing MPCS with AMM and MPCS with AL, it can be seen that the performance of MPCS with AMM is higher at all frequencies. This difference can be attributed to the fact that the parameters of the linear term of the system are not updated by AMM. Therefore, the effectiveness of adaptive model matching is confirmed once again.

6 Conclusions

A novel tracking controller design for a tap-water-driven McKibben-type artificial muscle is proposed by applying a model predictive control and the results of the analysis of the contribution of the system are shown. First, the McKibben muscle employing the asymmetric Bouc-Wen model is described, and an appropriate model with a high NRMSE is obtained experimentally. Next, a model predictive control based on a servomechanism is designed. An inverse optimization method is thereafter proposed to reduce the controller-tuning routines. However, this method requires solvability and calculation provided that the adaptive algorithm is applied. Therefore, the AMM is applied to match a closed-loop system to the prespecified LTI predictor in the model predictive controller, to overcome the aforementioned problem. The experimental results show that the proposed method is more robust to load and frequency changes than the conventional method. In particular, at 0.3 Hz, the performance is improved by 72% that demonstrates the effectiveness of the proposed method.

Eventually, the contribution of the system is analyzed by comparing the four control strategies, and the results show that the contribution of the adaptive system is much higher than that of the servo system. Therefore, the results show that MPC with AMM has a higher control performance than MPCS with AMM. In addition, the control performance of the MPCS with AL is degraded compared with that of the MPCS with AMM because it takes a longer time to reach the steady-state response; this confirms the effectiveness of the proposed adaptive model matching method once again.

The proposed control system is expected to be applied to a practical mechanical systems and robotics that require high cleanliness and high-precision control performance, taking advantages of the McKibben-type artificial muscles and the tap-water-drive system. In the future, the control system that admits the load variation during the experiment and does not require an exact mathematical model is constructed for expanding the range of applications.

Acknowledgements
We would like to thank Editage (www.editage.com) for English language editing.

Funding
Not applicable.

Availability of data and materials
The datasets used and/or analysed during the current study are available from the corresponding author on reasonable request.

Competing interests
The authors declare that they have no competing interests.

Authors' contributions
All the authors contributed immensely to the success of this study. ST contributed to doing the experiments and the discussion of the analysis, and to writing the paper. RI contributed to the theoretical works that are modeling for muscle and designed control systems. KI contributed to the discussion of the theoretical works, the analysis and the revision of the paper. All authors read and approved the final manuscript.

Authors' information
Satoshi Tsurhara is received the B.E. degree from Shibaura Institute of Technology, Japan, in 2021. He is currently in a master's program at Graduate school of Shibaura Institute of Technology, Japan. His current research interests include adaptive control and data-driven control of nonlinear system and its application in mechanical system, e.g., aqua drive system.

Ryo Inada received his M.E. degree from Graduate school of Shibaura Institute of Technology, Japan, in 2020. He is currently working at Hitachi Construction Machinery Co., Ltd., Japan. His research interests include controller design for nonlinear system and its application to mechatronics, especially in hydraulics systems.

Kazuhisa Ito received the B.E. and M.S. degrees from Sophia University, Japan, in 1993 and 1995, respectively. From 1995, he worked for Komatsu Ltd. He received the Ph.D. Degree in Mechanical Engineering from Sophia University, Tokyo, Japan, in 2001. Since 2001, he has been a faculty member as an Assistant Professor and then a lecturer in Department of Mechanical Engineering at Sophia University. Via an Associate Professor in Department of Mechanical Engineering, Tottori University, since 2011, he is a Professor in Department of Machinery and Control Systems, College of Systems Engineering and Science, Shibaura Institute of Technology. His current research interests include adaptive control theory of nonlinear systems, robust control theory and its applications in mechanical systems, e.g., fluid power systems, agriculture systems, aqua drive system etc.

Author details
[1]Graduate School of Mechanical Engineering, Shibaura Institute of Technology, 307 Fukasaku, Minuma, Saitama 3378570, Japan. [2]MEng Graduate School of Mechanical Engineering, Shibaura Institute of Technology, 307 Fukasaku, Minuma, Saitama 3378570, Japan. [3]Department of Machinery and Control Systems, Shibaura Institute of Technology, 307 Fukasaku, Minuma, Saitama 3378570, Japan.

References

1. Andrikopoulos, G., Nikolakopoulos, G., Manesis, S.: A Survey on applications of Pneumatic Artificial Muscles. In: Proceedings of the 19th Mediterranean Conference on Control and Automation, pp. 1439–1446 (2011)
2. Miyakawa, S.: Aqua Drive System : a technology using tap water and its applications Pro posing ADS to the markets. In: Proceedings of the 8th JFPS Internatioanl Symposium on Fluid Power, pp. 26–37 (2011)
3. Kobayashi, W., Dohta, S., Akagi, T., Ito, K.: Analysis and modeling of tap-water/pneumatic drive McKibben type artificial muscles. International Journal of Mechanical Engineering and Robotics Research **6**(6), 463–466 (2017)
4. Nouri, A.S., Gauvert, C., Tondu, B., Lopez, P.: Generalized variable structure model reference adaptive control of one-link artificial muscle manipulator in two operating modes. In: Proceedings of the IEEE International Conference on Systems, Man and Cybernetics, vol. 2, pp. 1944–1950 (1994)
5. Carbonell, P., Jiang, Z.P., Repperger, D.W.: Nonlinear control of a pneumatic muscle actuator: Backstepping vs. sliding-mode. In: Proceedings of the IEEE Conference on Control Applications, pp. 167–172 (2001)
6. Pujana-Arrese, A., Mendizabal, A., Arenas, J., Prestamero, R., Landaluze, J.: Modelling in Modelica and position control of a 1-DoF set-up powered by pneumatic muscles. Mechatronics **20**(5), 535–552 (2010)
7. Shen, X.: Nonlinear model-based control of pneumatic artificial muscle servo systems. Control Engineering Practice **18**(3), 311–317 (2010)
8. Wu, J., Huang, J., Wang, Y., Xing, K.: Nonlinear disturbance observer-based dynamic surface control for trajectory tracking of pneumatic muscle system. IEEE Transactions on Control Systems Technology **22**(2), 440–455 (2014)
9. Lin, C.J., Lin, C.R., Yu, S.K., Chen, C.T.: Hysteresis modeling and tracking control for a dual pneumatic artificial muscle system using Prandtl-Ishlinskii model. Mechatronics **28**, 35–45 (2015)
10. KOSAKI, T., SANO, M.: Control of a Parallel Manipulator Driven by Pneumatic Muscle Actuators Based on a Hysteresis Model. Journal of Environment and Engineering **6**(2), 316–327 (2011)
11. Aschemann, H., Schindele, D.: Comparison of model-based approaches to the compensation of hysteresis in the force characteristic of pneumatic muscles. IEEE Transactions on Industrial Electronics **61**(7), 3620–3629 (2014)
12. Wang, G., Chen, G., Bai, F.: Modeling and identification of asymmetric Bouc-Wen hysteresis for piezoelectric actuator via a novel differential evolution algorithm. Sensors and Actuators, A: Physical **235**, 105–118 (2015)
13. Inada, R., Ito, K., Ikeo, S.: Adaptive model predictive tracking control of tap-water driven muscle using hysteresis compensation with bouc-wen model. In: Proceedings of 16th Scandinavian International Conference on Fluid Power SICFP2019, pp. 3–3 (2019)
14. Inada, R., Ito, K., Ikeo, S.: Modeling and hysteresis compensation using asymmetric bouc-wen model for tap-water driven muscle and its application to adaptive model predictive tracking control. In: Proceedings of 15th International Conference on Fluid Control, Measurements and Visualization FLUCOME2019 (2019)
15. Ito, K., Inada, R.: Model predictive displacement control tuning of tap water driven muscle with adaptive model matching -numerical study-. In: Proceedings of The 2020 Bath/ASME Symposium on Fluid Power and Motion Control FPMC2020 (2020)
16. Tsuruhara, S., Inada, R., Ito, K.: Model predictive displacement control tuning for tap-water-driven muscle by inverse optimization with adaptive model matching. In: Proceedings of the 10th International Conference on Fluid Power Transmission and Control-ICFP2021, pp. 286–292 (2021)
17. Wei, Z., Xiang, B.L., Ting, R.X.: Online parameter identification of the asymmetrical Bouc-Wen model for piezoelectric actuators. Precision Engineering **38**(4), 921–927 (2014)
18. Cairano, S.D., Bemporad, A.: Model predictive control tuning by controller matching. IEEE Transactions on Automatic Control **55**, 185–190 (2009)
19. Mantri, R., Stoorvogel, A.A., Saberi, A.: Output regulation for linear discrete-time systems subject to input saturation. International Journal of Robust and Nonlinear Control **7**(11), 1009–1021 (1996)
20. Wada, N.: Model predictive tracking control for constrained linear systems using integrator resets. IEEE Transactions on Automatic Control **60**(11), 3113–3118 (2015)
21. Löfberg, J.: YALMIP: A toolbox for modeling and optimization in MATLAB. In: Proceedings of the IEEE International Symposium on Computer-Aided Control System Design, pp. 284–289 (2004)
22. Mattingley, J., Boyd, S.: CVXGEN: A code generator for embedded convex optimization. Optimization and Engineering **13**(1), 1–27 (2012)

Figures

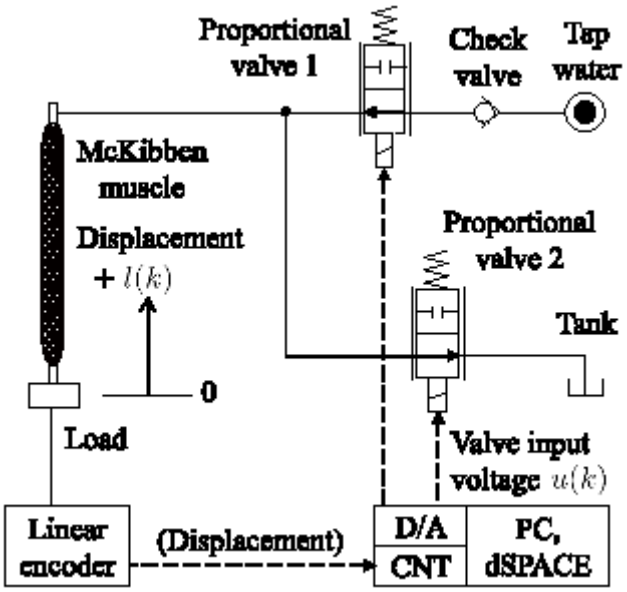

Figure 1

Experimental circuit

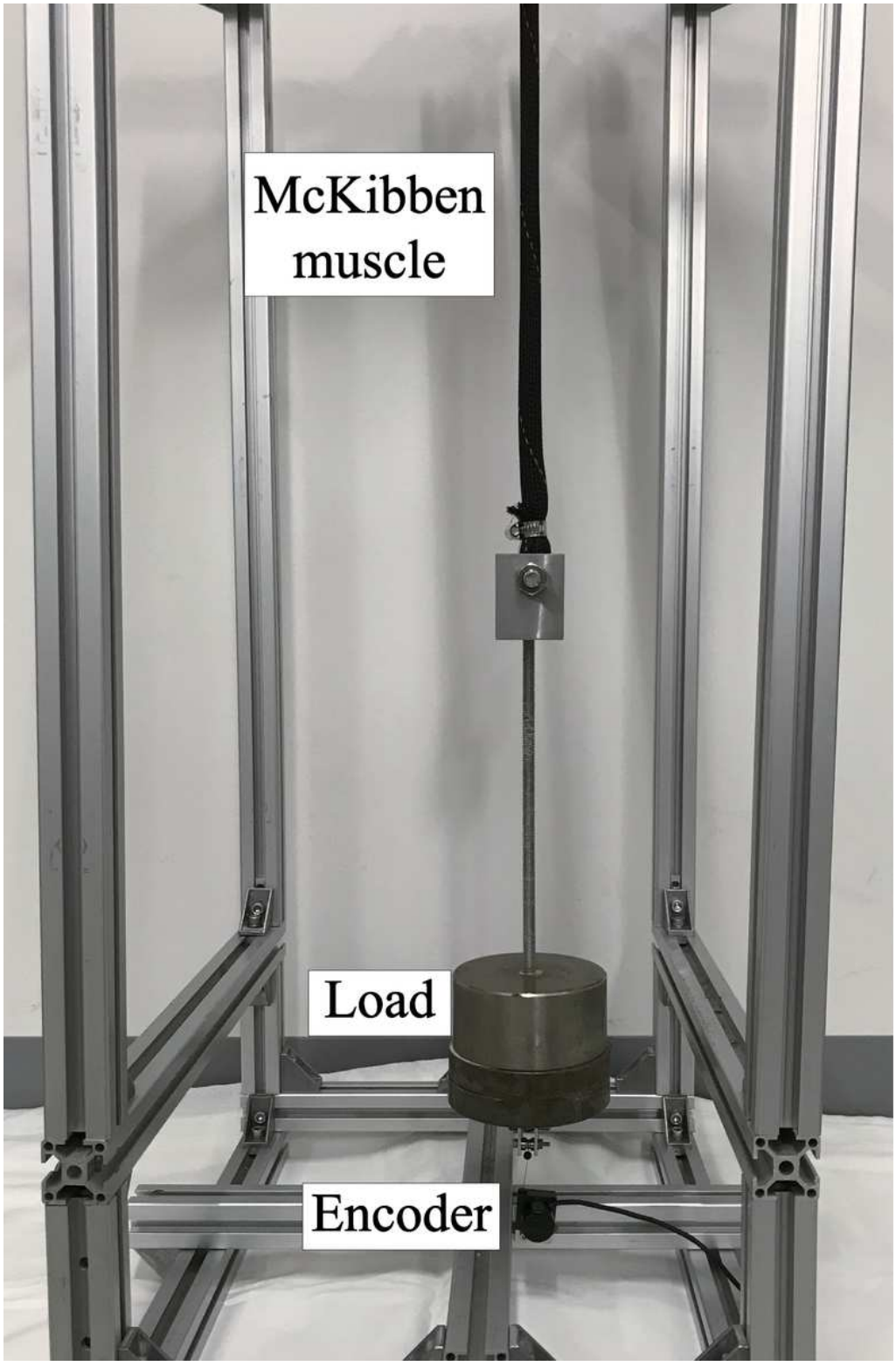

Figure 2

Experimental setup

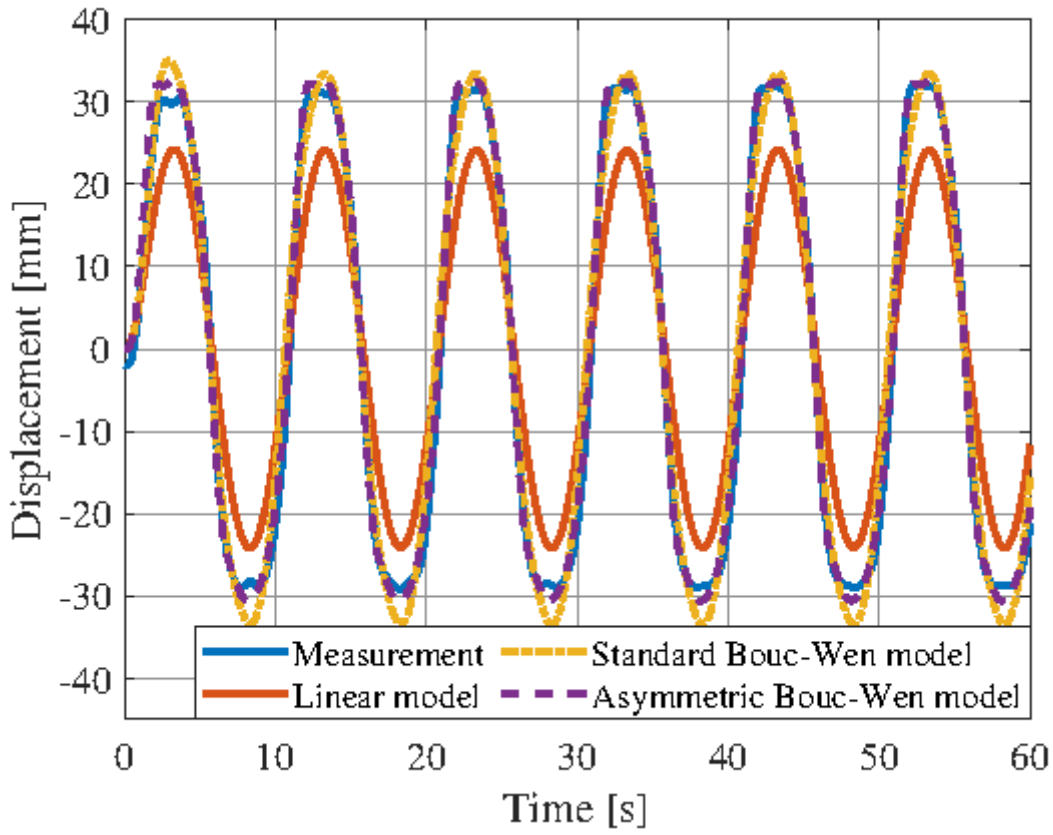

Figure 3

Comparison of temporal responses associated with each muscle model and the experimental results

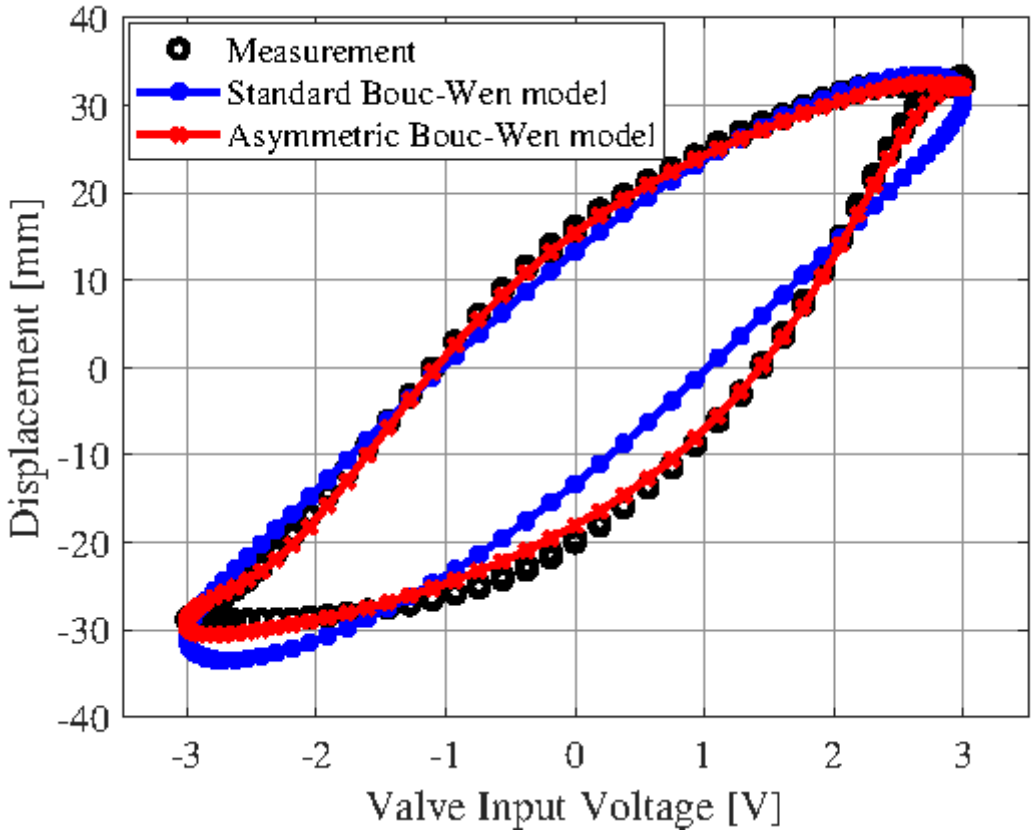

Figure 4

Comparison of hysteresis loop of each muscle model and the measurement results

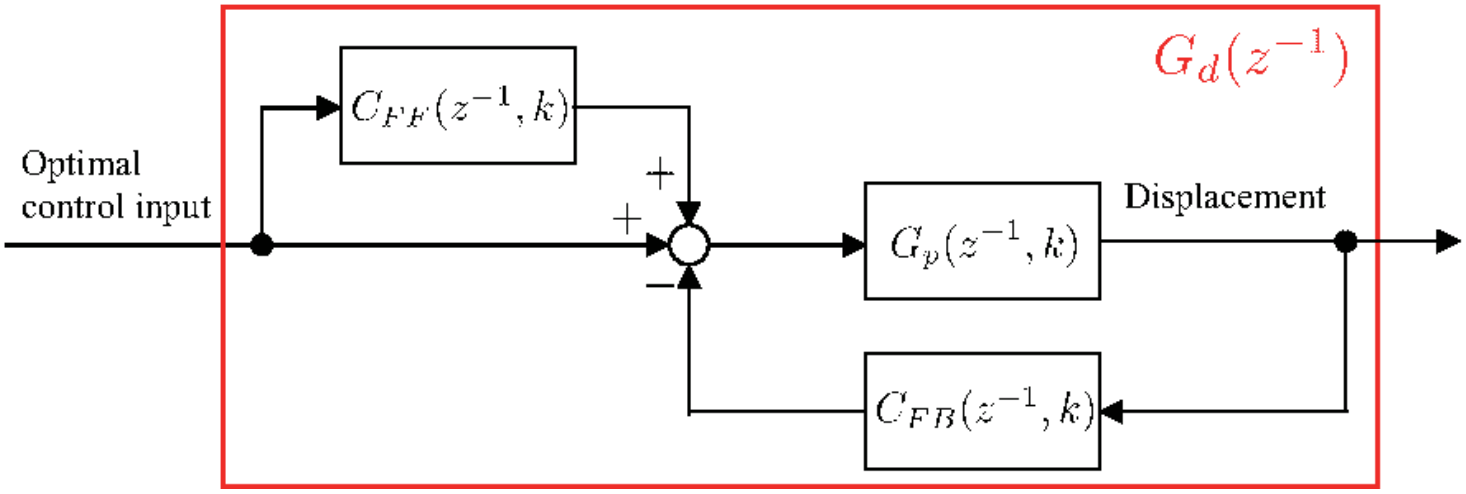

Figure 5

Conceptual schematic of adaptive model matching (AMM) compensator

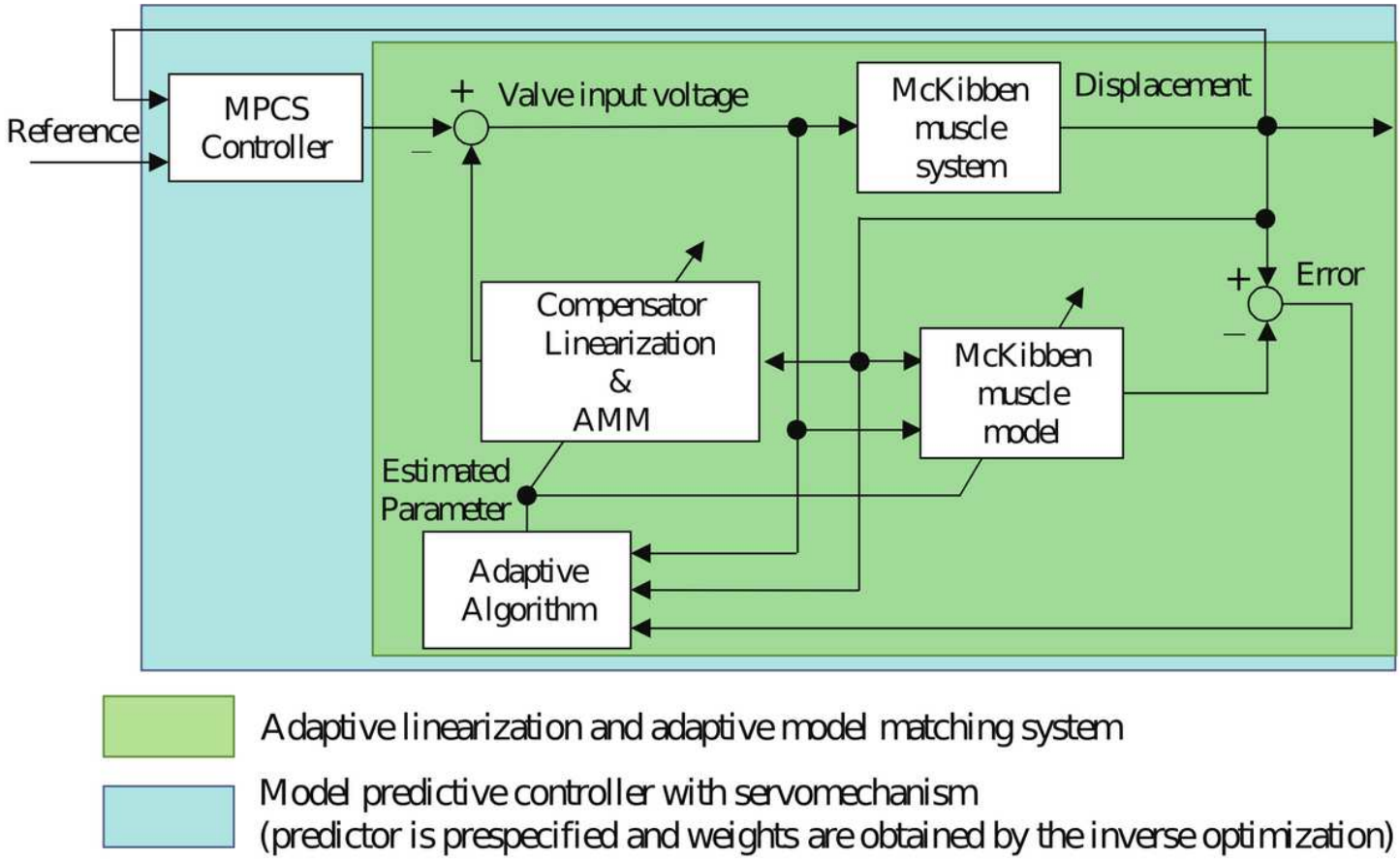

Figure 6

Block diagram of MPCS with AMM

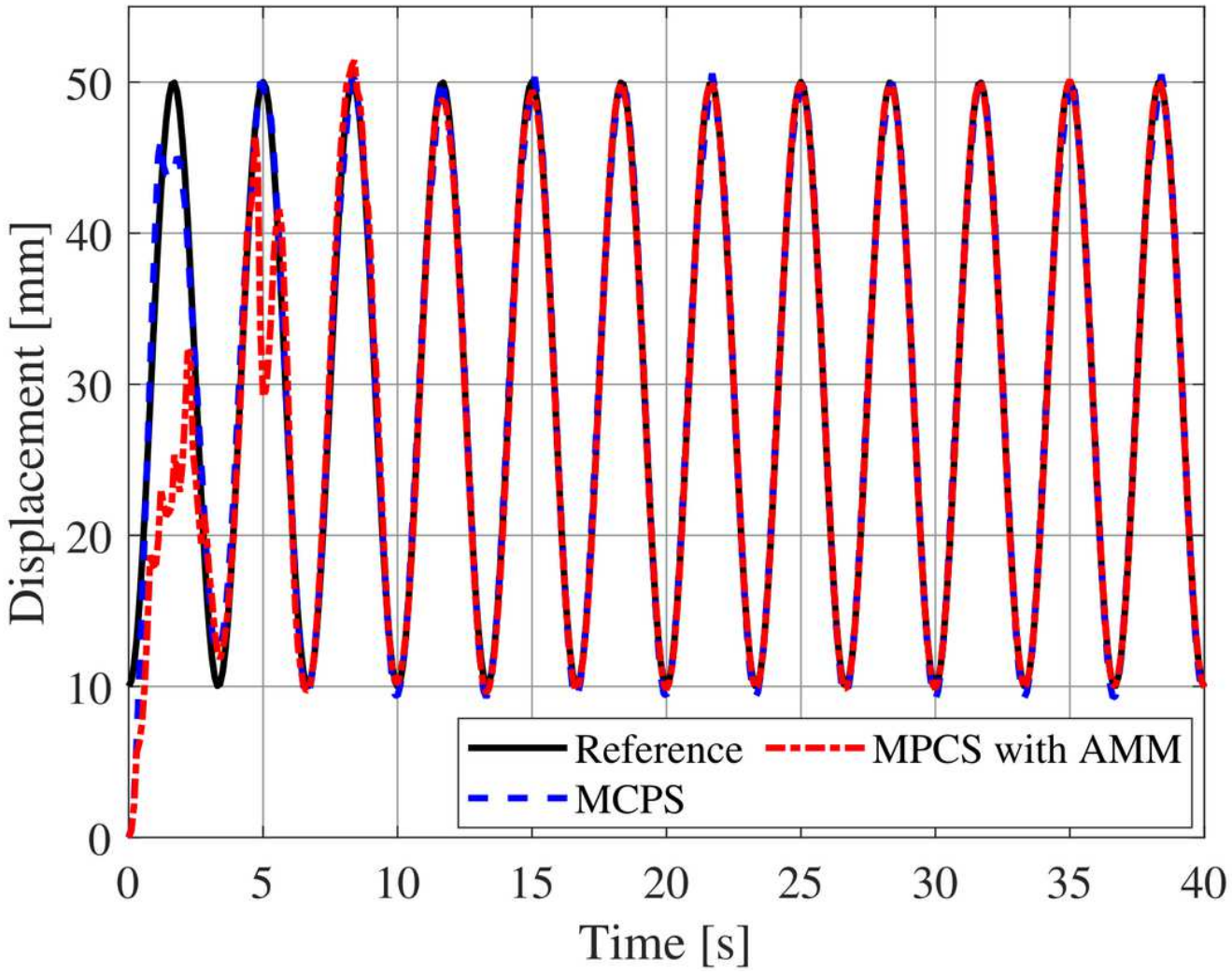

Figure 7

Comparison of tracking performances between MPCS with and without AMM

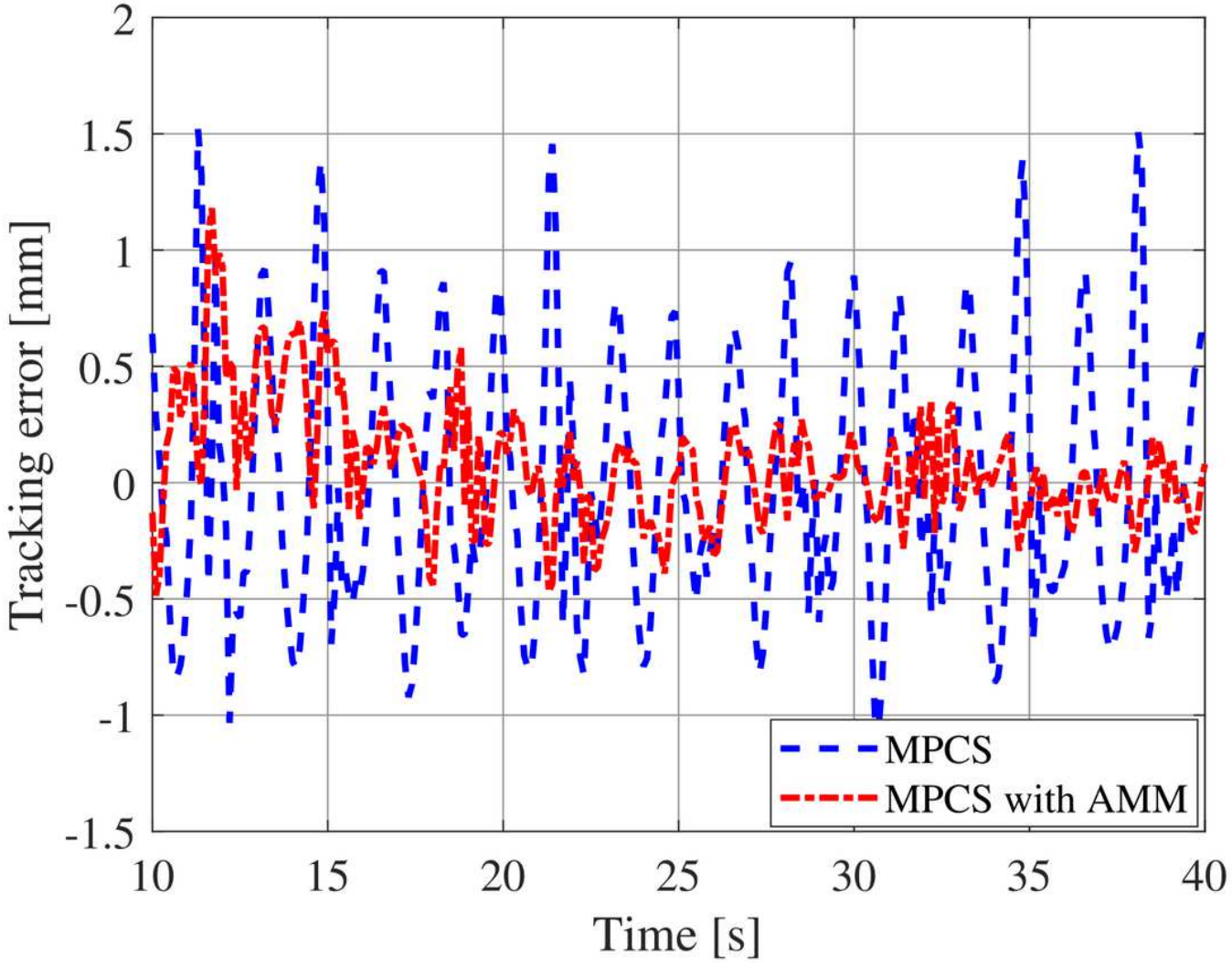

Figure 8

Comparison of tracking performances between MPCS and MPCS with AMM for the steady-state response

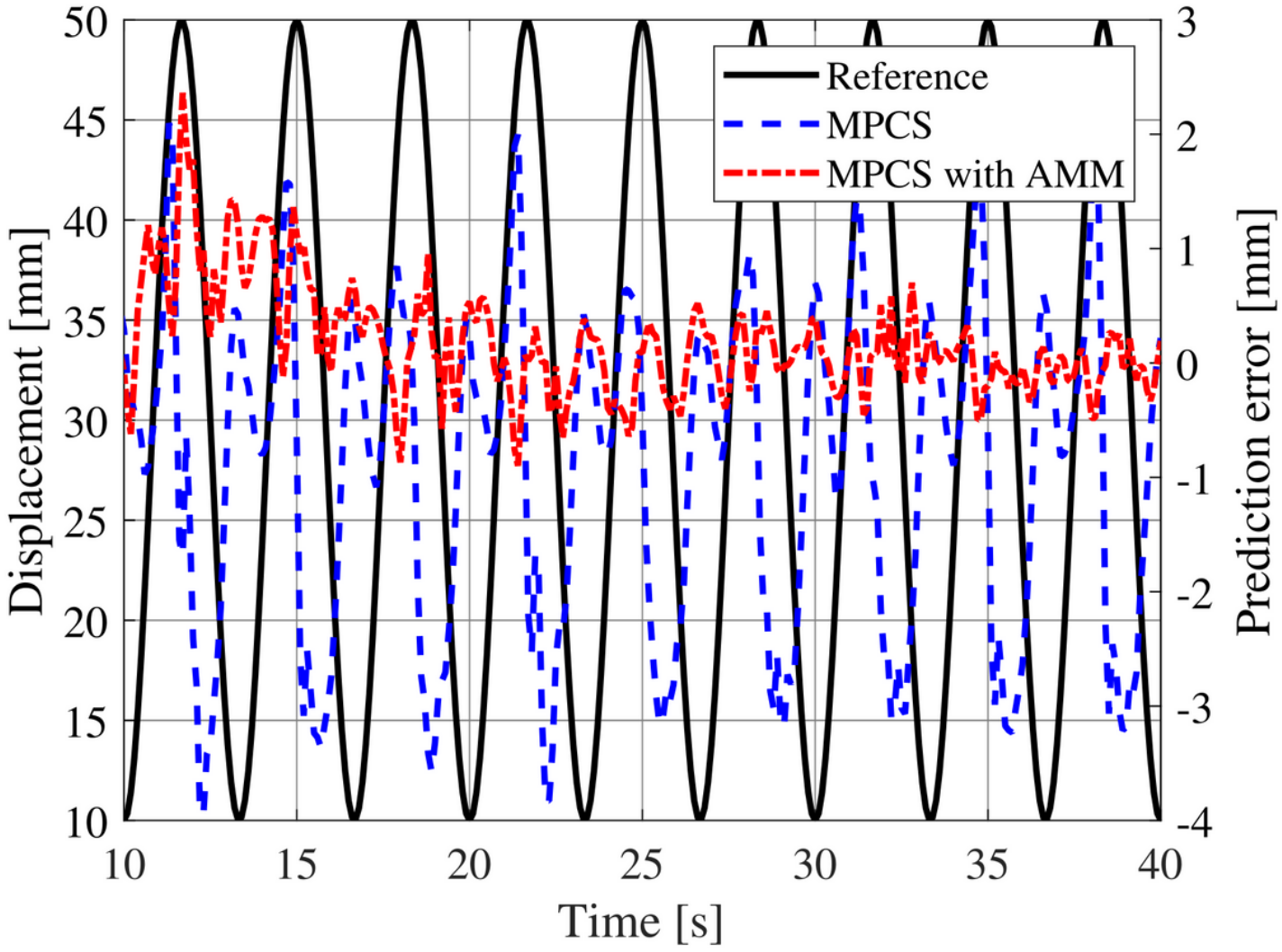

Figure 9

Comparison of prediction errors between MPCS with and without AMM for the steady-state response

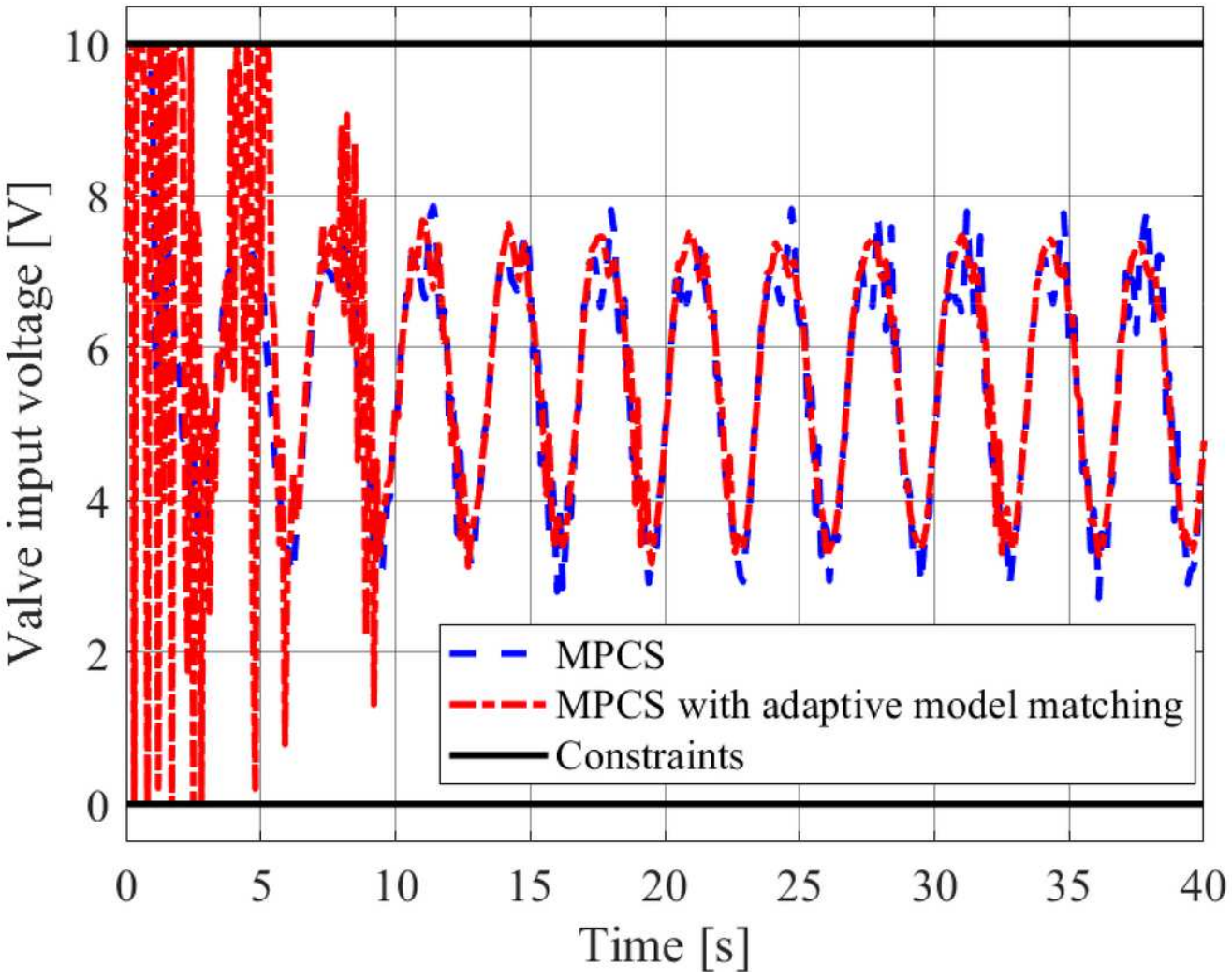

Figure 10

Comparison of control inputs between MPCS with and without AMM

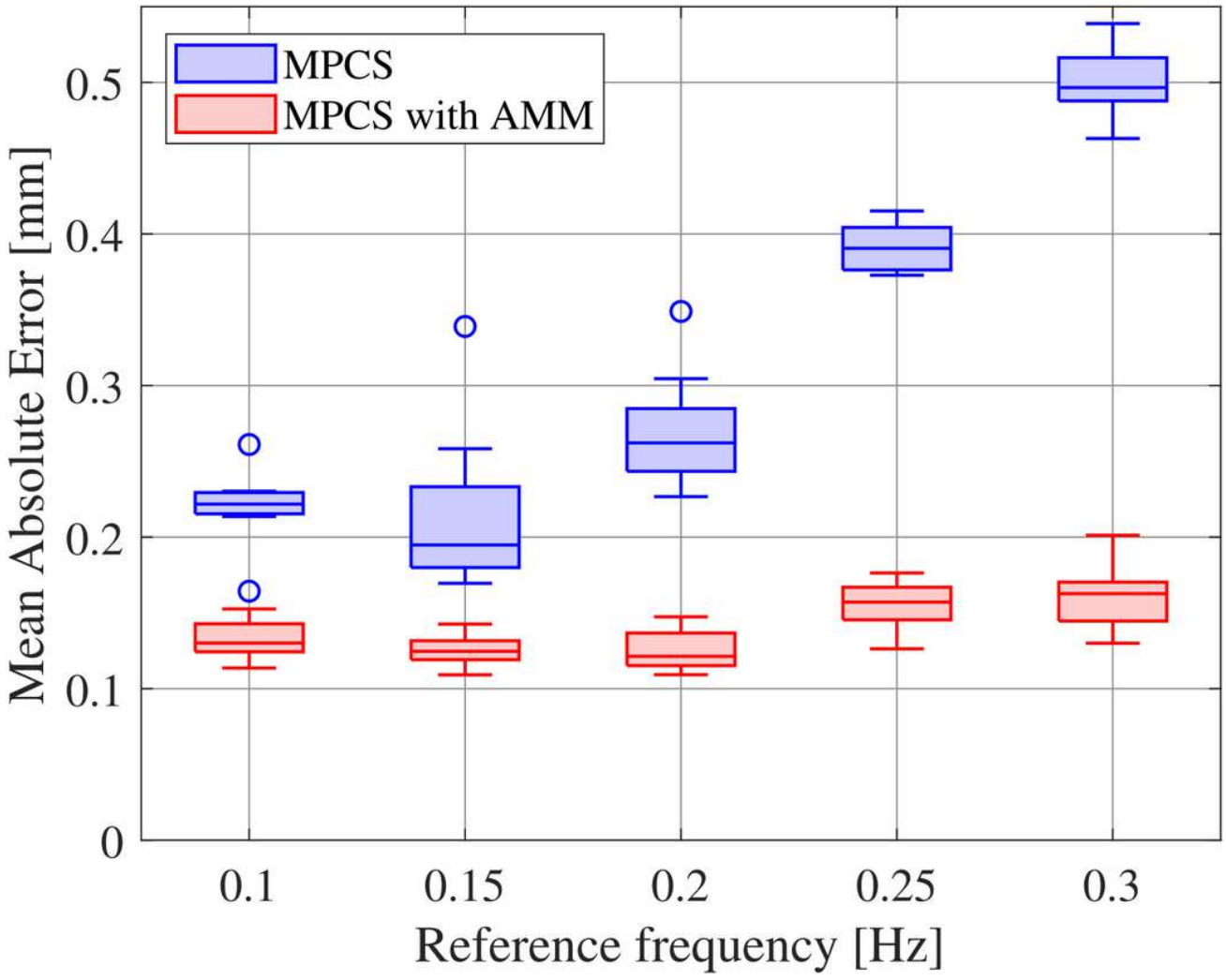

Figure 11

Comparison of box plots for MPCS and MPCS with AMM

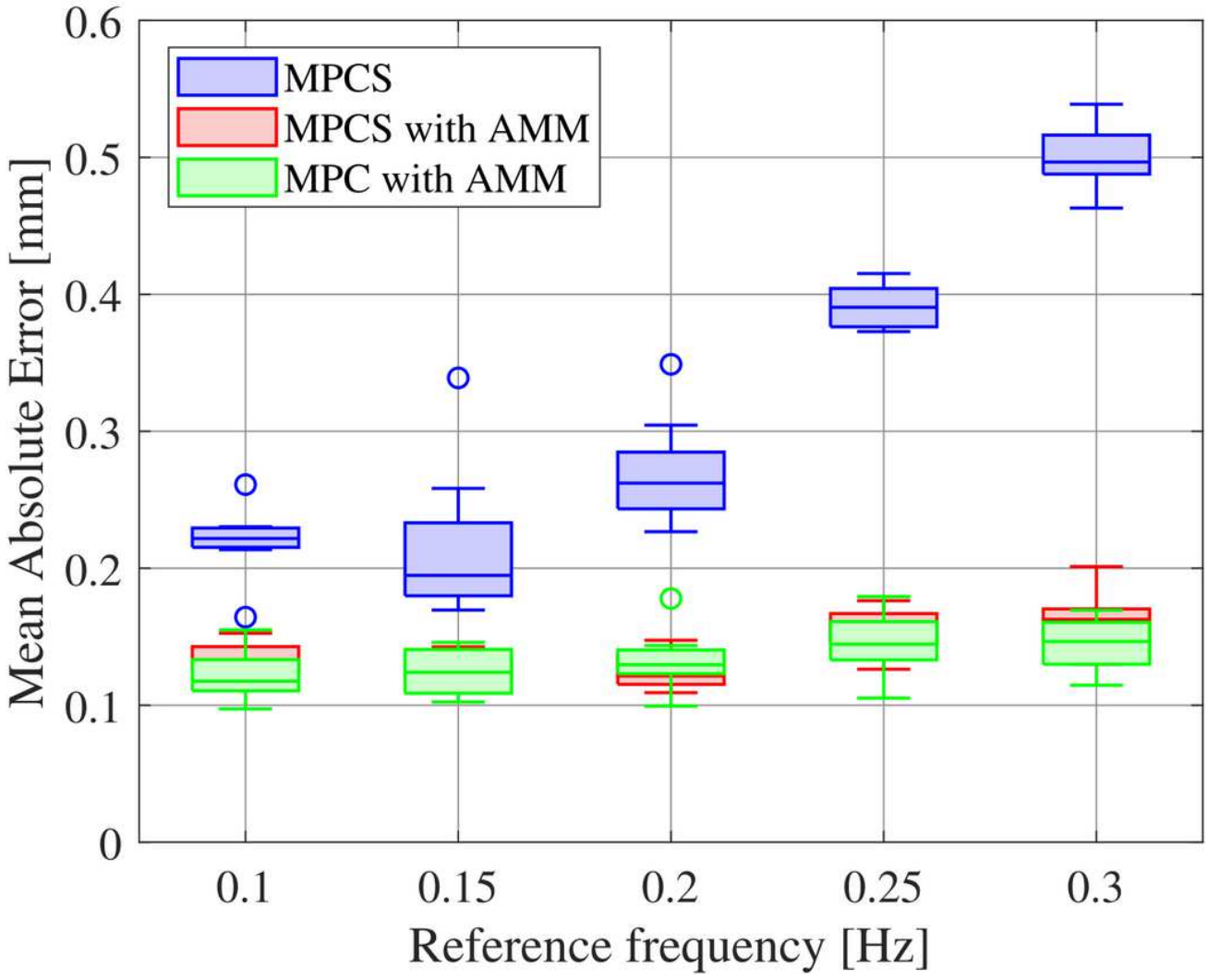

Figure 12

Comparison of box plots for investigating the contribution of servo and adaptive systems

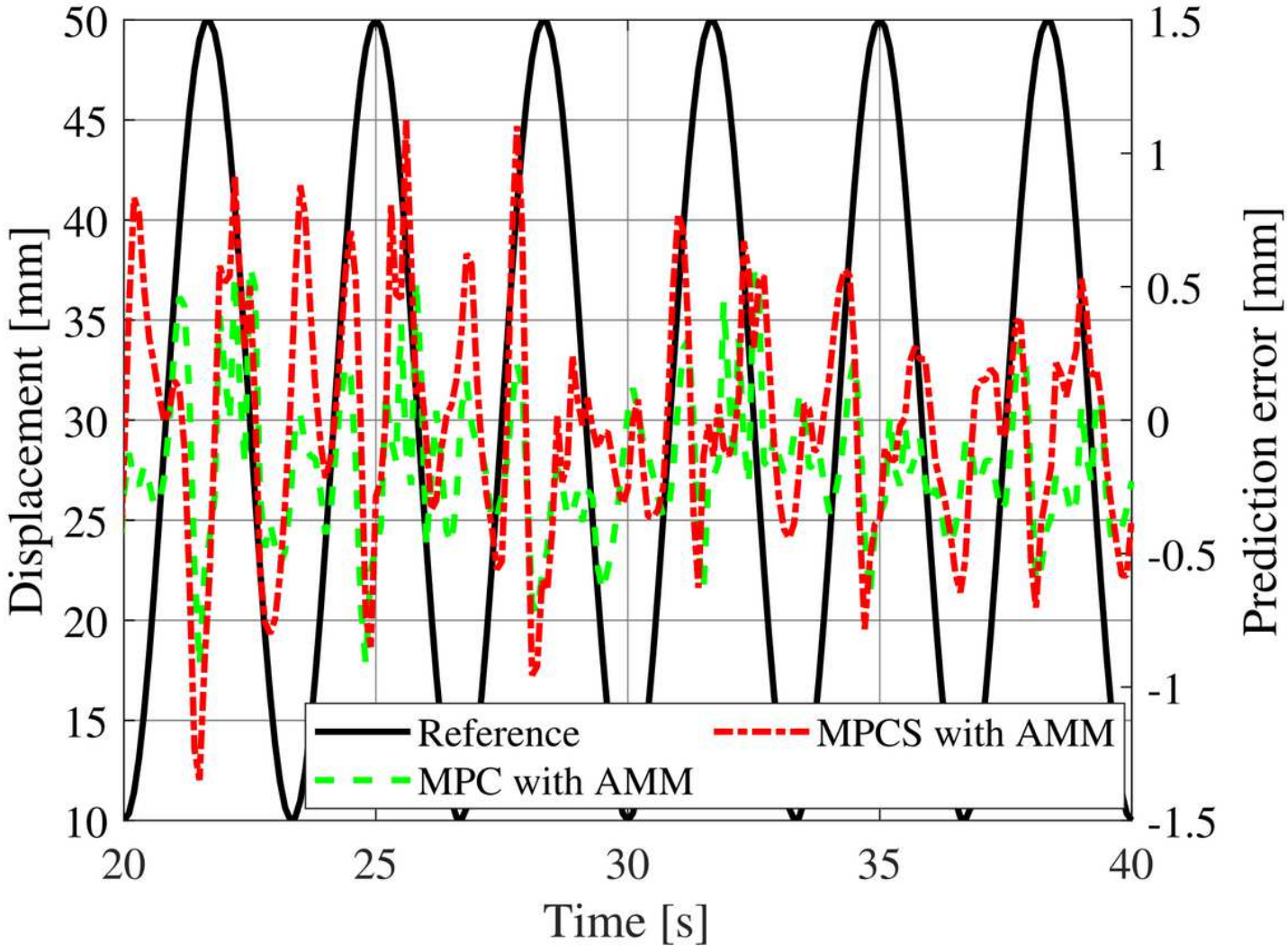

Figure 13

Comparison of prediction errors between MPCS with AMM and MPC with AMM

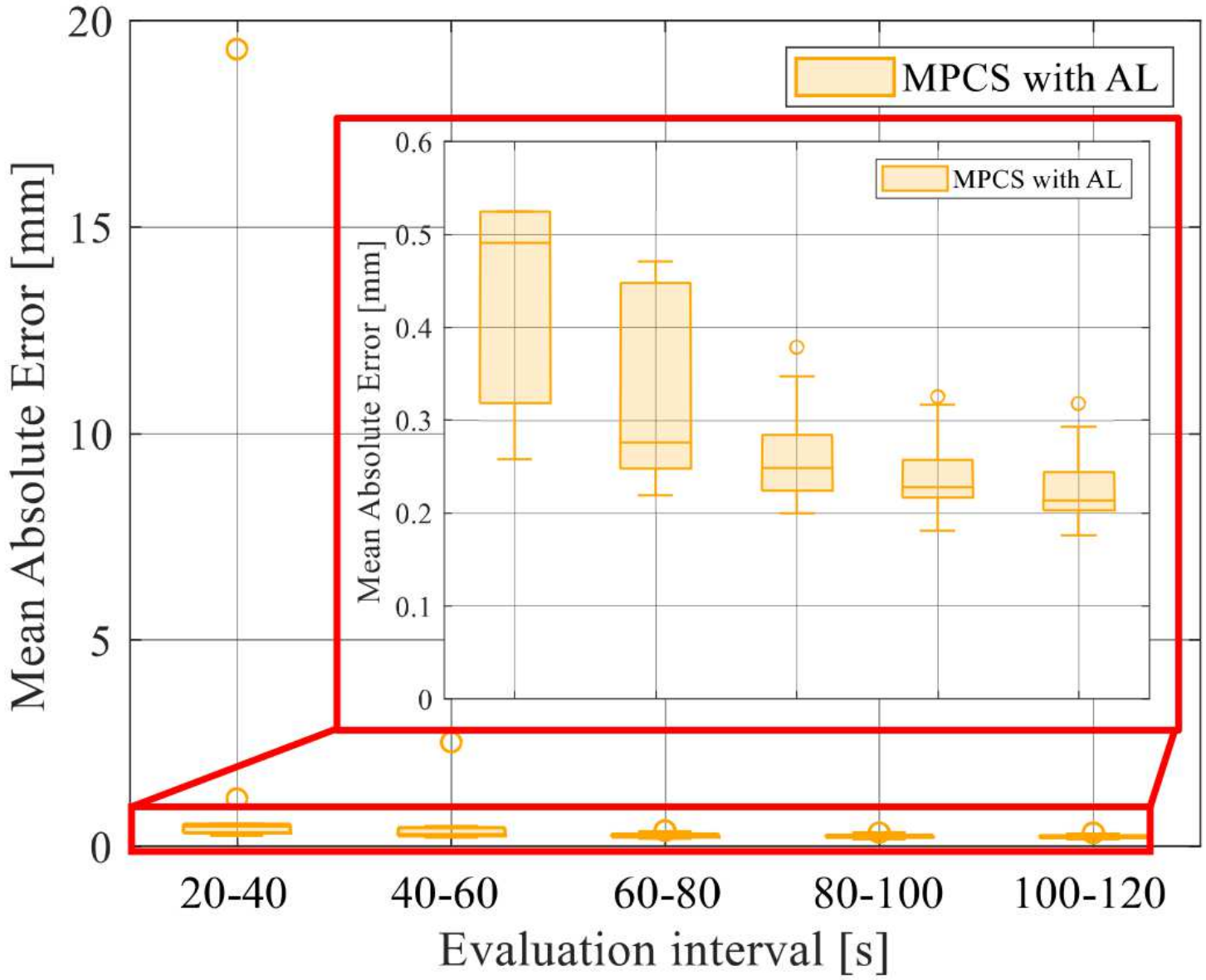

Figure 14

Comparison of MPCS with AL in each evaluation interval

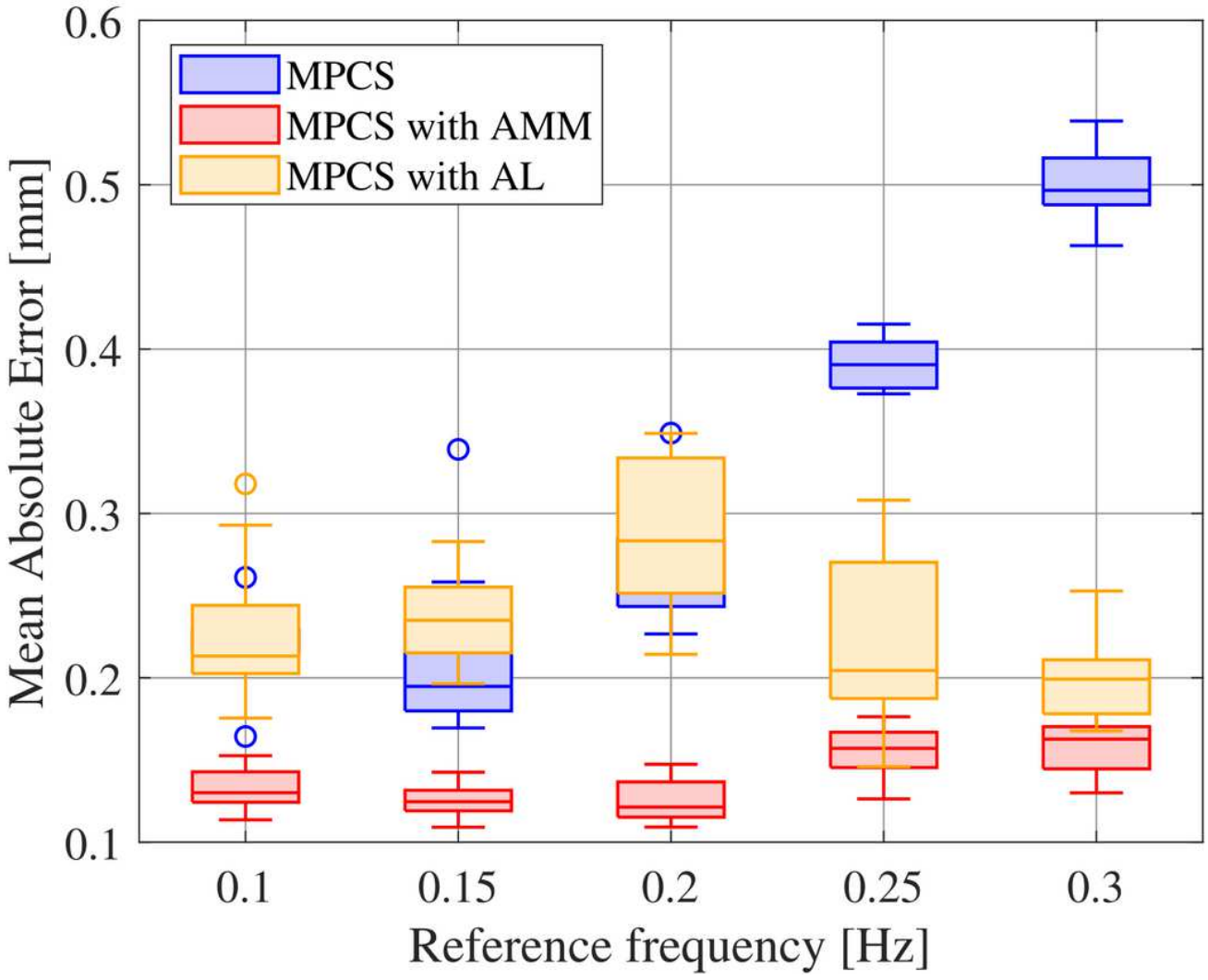

Figure 15

Comparison of box plots for evaluating the contribution of adaptive linearization and adaptive model matching